Leaf Area Index Variation for Crop, Pasture, and Tree in Response to Climatic Variation in the Goulburn–Broken Catchment, Australia

ZELALEM K. TESEMMA, YONGPING WEI, ANDREW W. WESTERN, AND MURRAY C. PEEL

Department of Infrastructure Engineering, University of Melbourne, Parkville, Victoria, Australia

(Manuscript received 25 June 2013, in final form 28 February 2014)

ABSTRACT

Previous studies have reported relationships between mean annual climatic variables and mean annual leaf area index (LAI), but the seasonal and spatial variability of this relationship for different vegetation cover types in different climate zones have rarely been explored in Australia. The authors developed simple models using remotely sensed LAI data from the Moderate Resolution Imaging Spectroradiometer (MODIS) and gridded climatic data from the Australian Water Availability Project. They were able to relate seasonal and annual LAI of three different land cover types (tree, pasture, and crop) with climatic variables for the period 2000–09 in the Goulburn–Broken catchment, Australia. Strong relationships were obtained between annual LAI of crop, pasture, and tree with annual precipitation (R^2 = 0.70, 0.65, and 0.82, respectively). Monthly LAI of each land cover type also showed a strong relationship (R^2 = 0.92, 0.95, and 0.95) with the difference between precipitation P and reference crop evapotranspiration (PET; P − PET) for crop, pasture, and tree. Independent model calibration and validation showed good agreement with remotely sensed MODIS LAI. The results from the application of the developed model on the future impact of climate change suggest that under all climate scenarios crop, pasture, and tree showed consistent decreases in mean annual LAI. For the future climate change scenarios considered, crop showed a decline of 7%–38%, pasture showed a decline of 5%–24%, and tree showed a decline of 2%–11% from the historical mean annual. These results can be used to assess the impacts of future climatic and land cover changes on water resources by coupling them with hydrological models.

1. Introduction

Leaf area index (LAI) is the ratio of the total one-sided area of leaf tissue per unit ground surface area. It is an important ecohydrological parameter for understanding the pathways and feedbacks between climate and vegetation and for improving agricultural water management in a wide range of regions (Arora 2002a; Donohue et al. 2006; Ge 2009; Groenendijk et al. 2011; Nielsen et al. 2012; O'Grady et al. 2011; Ramirez-Garcia et al. 2012; Wang et al. 2005; White et al. 2010; Zhang and Walsh 2007). Changing LAI modifies the water and energy budget of a surface by altering the number of stomatal openings and the surface albedo, which in turn affect biochemical and hydrological cycles (Negrón Juárez et al. 2009; Wang et al. 2005). From a management perspective, the relationship can be used when assessing the impacts of different policy options such as afforestation, deforestation, vegetation rehabilitation, and changed cropping on water yield, deep drainage, and salinity of a catchment (Palmer et al. 2010; Peel et al. 2010; Zhang et al. 2011; Zhao et al. 2012) and when assessing potential impacts of future climatic (Arora 2002b; Gilgen and Buchmann 2009; Peel 2009).

Despite its importance, accurately modeling LAI is challenging as many factors, such as the availability of nutrients and water and management practices including cropping, harvesting, application of fertilizer, and revegetation, all affect LAI (Donohue et al. 2006). In areas where water is the main limiting factor, LAI is highly dependent on water availability (Zhang et al. 2004), so a strong relationship between LAI and climate can occur (Donohue et al. 2006). Most previous work has considered the Normalized Difference Vegetation Index (NDVI), which is calculated by dividing the difference of near-infrared radiation (NIR) and visible radiation (VIS) by the sum of NIR and VIS from satellite image products. Both NDVI and LAI have been derived from a range of satellite sensors including the Advanced Very High Resolution

Corresponding author address: Yongping Wei, Department of Infrastructure Engineering, University of Melbourne, Grattan Street, Parkville, VIC 3010, Australia.
E-mail: ywei@unimelb.edu.au

DOI: 10.1175/JHM-D-13-0108.1

Radiometer (AVHRR), the Moderate Resolution Imaging Spectroradiometer (MODIS), and various Landsat-based sensors over time. They have also been derived from field studies. The MODIS sensor operated on board the *Terra* (since 2000) and *Aqua* (since 2002) satellites provides MODIS-derived LAI data to the public. MODIS has 36 spectral bands with a spatial resolution of 250 m to 1 km and is designed to provide coverage of global vegetation conditions in fine detail. Based on AVHRR- and MODIS-derived products, a strong response between NDVI of boreal mixed wood forest and temporal climate variability was documented in Canada (Jahan and Gan 2011). Other studies have shown precipitation controls the annual and seasonal variation of the NDVI in Africa (Chamaille-Jammes et al. 2006; Richard and Poccard 1998) and North America (Wang et al. 2001). Using MODIS-derived LAI, Palmer et al. (2010) related LAI to mean annual aridity index for forest, woodland, and shrubland in Australia. Using ground-based LAI data, the LAI response of natural eucalypt forests in Australia to average annual climate (precipitation, potential evaporation, and temperature) has been reported (Ellis and Hatton 2008; O'Grady et al. 2011; Palmer et al. 2010; White et al. 2010).

Intercomparison of the various studies has shown that the LAI responses of each vegetation type to climatic variables differ because of differences in their function, structure, and distribution (Negrón Juárez et al. 2009). Therefore, a model that can predict spatially varying LAI at a monthly time scale using both precipitation and potential evapotranspiration, which also vary spatially, under different landscape and climate regions is critical for modeling carbon, water, and energy cycle at the catchment scale. A model that describes the spatial varying of LAI of different vegetation cover types at reasonable spatial and temporal scales could be incorporated into hydrological models that then help us understand the impacts of climatic changes and land use and land cover changes on runoff in catchments.

The aims of this paper are to 1) examine the spatiotemporal relationships between LAI of crop, pasture, and tree and climatic variables; 2) develop a simple model that describes spatiotemporal variability of LAI from spatiotemporal variable climatic inputs; and 3) assess future climate change impacts on LAI through projected changes in climatic variables. The Goulburn–Broken catchment, Australia, which includes three main land cover types (crop, pasture, and tree), is taken as the case study. Using MODIS product and ancillary data for 2000–09, statistical relationships between seasonal and annual climatic variables and LAI obtained by remote sensing of the three dominant land cover types on a pixel by pixel basis will be investigated.

2. Materials and method

a. Study area

The Goulburn–Broken catchment is located in Victoria, southeastern Australia, and is part of the Murray–Darling basin (MDB). The geographic location of the Goulburn–Broken catchment spans 35.8°–37.7°S in latitude and 144.6°–146.7°E in longitude, with a total catchment area of 24 000 km^2 (Fig. 1a). The catchment elevation ranges from a maximum altitude of about 1790 m MSL on the southern side of the catchment to a minimum altitude of about 86 m MSL on the northern side of the catchment.

The catchment has marked differences in climate from south to north. According to the Köppen–Geiger climate classification, the Goulburn–Broken catchment includes three climatic zones; from the northwest corner to the southeast corner of the catchment, these are semiarid (BSk, 9%); without dry season, hot summer temperate (Cfa, 35%); and without dry season, warm summer temperate (Cfb, 55%; Peel et al. 2007). The precipitation in the catchment is influenced by mountain ranges with high precipitation in the southern part and flat plains in the northern part with declining precipitation as one moves from south to north. The mean annual precipitation (2000–09) is 1476 mm yr^{-1} in the southern mountainous part, decreasing to approximately 322 mm yr^{-1} in the flat northern part of the catchment (Fig. 1b). The mean annual temperature (2000–09) varies from 7.1° to 16.5°C (Fig. 1c) with a mean daily maximum of 23.5°C in summer and a mean daily minimum of 1°C in winter. The mean annual reference crop evapotranspiration (Fig. 1d) for the same period varies from 807 mm yr^{-1} in the southeast to 1287 mm yr^{-1} in the northern part of the catchment, following the spatial pattern of the mean annual temperature.

The Goulburn–Broken catchment is covered by three dominant land cover types: crop, pasture, and tree (Fig. 1e). Large-scale changes in vegetation cover started in Australia after European settlement with the expansion of cropland (Gordon et al. 2003). Before European settlement, the Goulburn–Broken catchment was covered with grassland, woodland, and tree. Tree and woodland clearing for agriculture started during the nineteenth century, and clearing expanded for pasture development beginning in the 1950s and reached a maximum in the 1970s (Graetz 1998). The current land cover shows most of the southern part of the catchment is covered by tree, mainly eucalyptus open tall trees and eucalyptus woodlands, whereas cropland is located in the northern part of the catchment.

b. Datasets and analysis

All climate data used in this study, except the average daily wind speed, are from the Australian Water

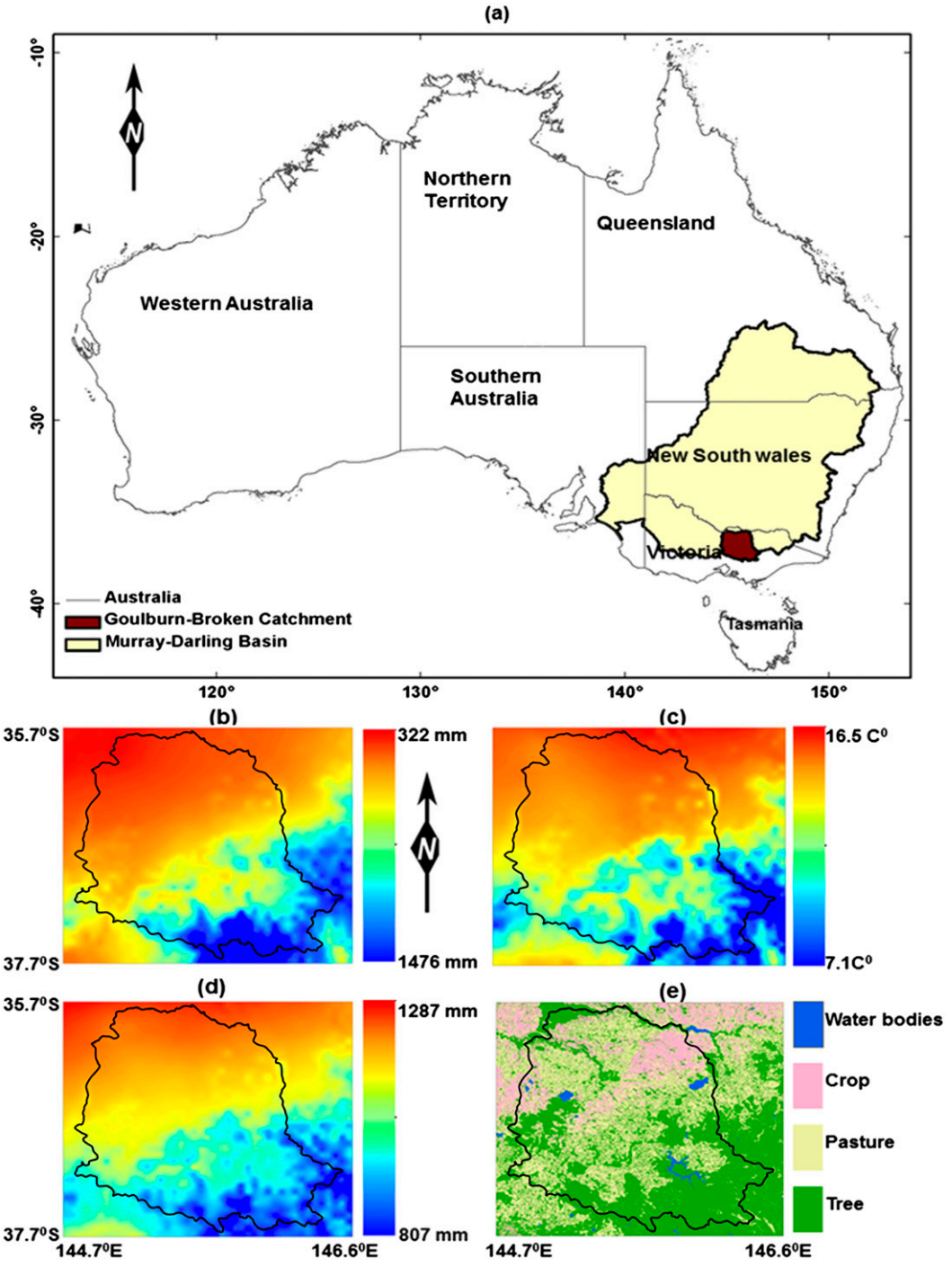

FIG. 1. (a) Location map of the Goulburn–Broken catchment in Australia, (b) mean annual precipitation (mm), (c) mean annual temperature (°C), (d) mean annual reference crop evapotranspiration (mm) for the period 2000–09, and (e) spatial distribution of land cover types (water bodies, crop, pasture, and tree) in the study area.

Availability Project (AWAP) dataset, which provides spline-interpolated point data (Jones et al. 2007, 2009). The average daily wind speed data were obtained from McVicar et al. (2008) and are also based on spline-interpolated point data. The data used in this study cover the period from January 1999 to December 2009. The spatial resolution of the daily precipitation (mm), daily maximum and minimum temperature (°C), actual vapor pressure (hPa), daily incoming solar radiation (MJ m^{-2}), and average daily wind speed (m s^{-1}) is

0.05° × 0.05° (approximately 5 km × 5 km). The 9-s spatial resolution elevation (m) data were obtained from Geoscience Australia (2008) and resampled to 0.05° × 0.05° using the average aggregation method in ArcGIS.

The daily climate data were summed or averaged into monthly and annual values on a pixel by pixel basis for further analysis. In this study, monthly average reference crop evapotranspiration (PET, mm day^{-1}) was estimated using the Food and Agriculture Organization (FAO-56) Penman–Monteith method [see Eq. (1) and Allen et al. (1998)] and monthly average data. Total monthly reference crop evapotranspiration was calculated by multiplying the average monthly reference crop evapotranspiration estimate by the number of days of the respective month (Allen et al. 1998):

$$\mathrm{PET} = \frac{0.408\Delta(R_n - G) + \gamma \dfrac{900}{T_a + 273} u_2(\theta_S - \theta_a)}{\Delta + \gamma(1 + 0.34u_2)}, \quad (1)$$

where Δ is the slope of the vapor pressure curve (kPa °C^{-1}) at air temperature; R_n is the average monthly net radiation at the grass surface (MJ m^{-2} day^{-1}); G is the soil heat flux (MJ m^{-2} day^{-1}), which can be estimated using Allen et al. (1998) as $G = 0.14\ (T_i - T_{i-1})$ for monthly calculation where T_i and T_{i-1} are the average monthly air temperatures (°C) for month i and $i - 1$, respectively; γ is the psychrometric constant (kPa °C^{-1}); T_a is the average monthly mean temperature (°C); u_2 is the average monthly wind speed (m s^{-1}) at 2-m height; and $e_s - e_a$ is the average monthly saturation vapor pressure deficit (kPa). This study adopted the properties of the FAO-56 hypothetical crop of assumed height of 0.12 m, a surface resistance of 70 s m^{-1}, and an albedo of 0.23 (Allen et al. 1998; McMahon et al. 2013).

The land cover map for the Goulburn–Broken catchment was extracted from the MODIS dynamic land cover product MCD 12Q2.005, which is available from the MODIS website (http://modis.gsfc.nasa.gov/data/dataprod/index.php). These products provide the annual land cover type from 2001 through 2009 at a spatial resolution of approximately 500 m × 500 m. First, we grouped similar vegetation into three dominant land cover types (crop, pasture, and tree) in the catchment. Tree comprised about 48%, pasture and grass occupied 39%, crop covered about 12%, and water bodies cover 1% of the catchment area. The annual time series of the three dominant land cover maps from 2000 to 2009 were then derived for each MODIS pixel. The LAI data were downloaded from the Beijing Normal University (BNU; available from http://globalchange.bnu.edu.cn). This dataset was created with an improved retrieval algorithm to reduce uncertainties that arise from cloud, snow, and instrument problems in the MOD15A2 LAI products (Yuan et al. 2011). The retrieval process for MOD15A2 LAI values relies on two algorithms, the main and the backup. The three-dimensional radiative transfer model generates several spectral and angular signatures that can be compared to the MODIS directional surface reflectance values through a lookup table for different sets of canopy realization and leaf architecture views. Further documentation of the theoretical background and mathematical derivation of the main algorithm can be found in Knyazikhin et al. (1998). The second, or backup, algorithm is a set of regression curves [see Eq. (2)] between LAI and NDVI for different biomes that are activated when the main algorithm fails (Yuan et al. 2011):

$$\mathrm{LAI} = f(\mathrm{NDVI}), \quad (2)$$

where f is the nonlinear regression curve between LAI and NDVI (Fig. 2) for different biomes and NDVI is calculated by dividing the difference of NIR and VIS by the sum of NIR and VIS:

$$\mathrm{NDVI} = \frac{\mathrm{NIR} - \mathrm{VIS}}{\mathrm{NIR} + \mathrm{VIS}}. \quad (3)$$

An NDVI value of zero indicates no green leaves and a value close to +1 indicates densely green leaves. The difference between the two algorithms is reported as a quality control layer, which helps users to assess the accuracy of the retrieval. Better results are obtained when the LAI is estimated from the main algorithm (Yuan et al. 2011).

The BNU MODIS LAI dataset is a composite LAI from January 2000 to December 2009 at 8-day intervals at a spatial resolution of 0.0083° × 0.0083° (approximately 1 km × 1 km). The monthly LAI was calculated by taking the weighted average based on the number of days that contributed to that 8-day-interval LAI. The BNU MODIS LAI has 46 images per year, which start on the first day of the year and continue to the 361st day of that year. Detailed information on the reprocessing procedure and its validation can be found in Yuan et al. (2011). The quality of MOD15A2 LAI dataset for Australia has been assessed in previous works (Coops et al. 2012; Fang et al. 2012; Fuentes et al. 2008; Guindin-Garcia et al. 2012; Hill et al. 2006; Sea et al. 2011). Their results suggest MOD15A2 LAI product is in good agreement with ground-based measurements of canopy LAI at different sites in Australia. A comparison between the original MOD15A2 LAI and BNU MODIS LAI in our study area showed that they are the same except for some improvement in some months (not shown).

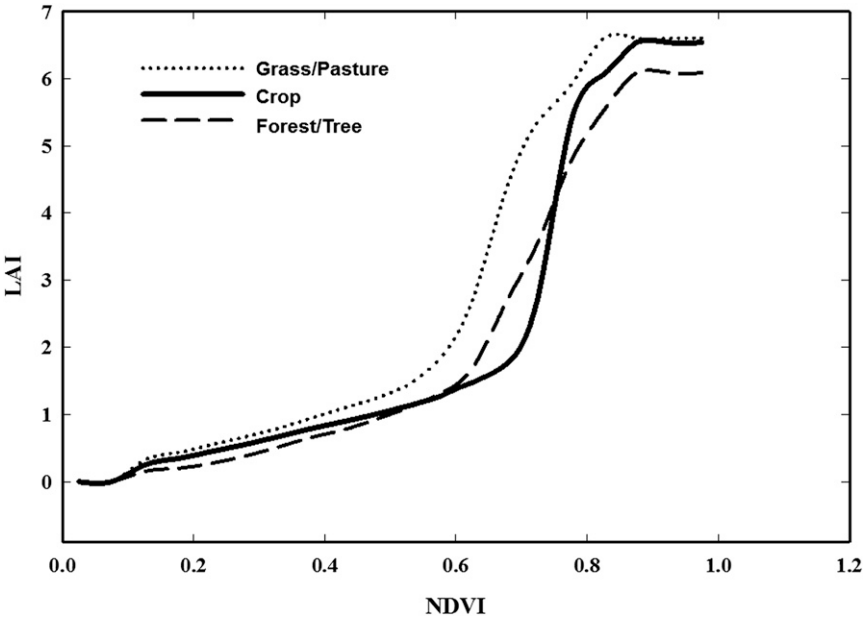

FIG. 2. Relationships between NDVI and LAI of crop, grass/pasture, and tree, which are used to estimate LAI from NDVI as implemented in MODIS backup algorithm (reproduced from Knyazikhin et al. 1999).

To establish relationships between LAI and climatic variables for a given land cover type, the mismatch in spatial resolutions among the land cover type, BNU MODIS LAI, and AWAP climatic data was resolved in the following way. If the LAI pixel fell completely within an AWAP pixel, then the LAI pixel was assigned the climatic variable value of that AWAP pixel (Figs. 3a,c). Otherwise, the area-weighted average of the climatic variable for all AWAP pixels that intersected the LAI pixel was taken. The percentage of each land cover type in the respective BNU MODIS LAI pixel was first calculated from the annual land cover type map (Fig. 3b). Where one land cover type dominates (>80%) the LAI pixel, the LAI value of that pixel was assigned to that cover (Figs. 3c,d), in case where the BNU MODIS LAI pixels that contain water bodies such as rivers or reservoirs and irrigation were removed from our sample to avoid the effect of additional water supply. The above processing avoided the problem of land cover type heterogeneity in the LAI calculations.

c. *Modeling LAI–climate relationships*

The annual and monthly LAI of the three vegetation types were regressed against the annual and the 1–12-month moving average of precipitation P, mean temperature T, reference crop evapotranspiration PET, and precipitation minus reference evapotranspiration (P − PET) here after moisture state on a pixel by pixel basis. All annual and monthly LAI values for each of the cover types for the period 2000–09 were used in developing the relationships. The time lags for the moving average that gave the strongest relationship using the coefficient of determination were selected during preliminary analysis. The seasonal variation of crop and pasture LAI was explained best with 6- and 9-month moving averages of moisture state (P − PET). Because of many LAI pixels (1 km × 1 km) falling within one climate pixel (5 km × 5 km), the plot of LAI against its respective explanatory climatic variables shows vertical scatter. Hence, the moisture state was grouped into bins of widths of 0.0928, 0.1069, and 0.1079 mm for crop, pasture, and tree, respectively, using Botev et al. (2010), and the average LAI of each bin was calculated. The effect of the bin width was assessed by increasing and decreasing the bin width calculated from Botev et al. (2010) and was found to have little effect on the regression analysis. The regression was then made between the bin-averaged LAI and the bin average of the climate variable. Based on scatterplots of the data, a feasible model was selected for the relationship between climate variables and LAI. The preliminary curve fitting was conducted on the following linear and nonlinear models, and the best performing model (the largest coefficient of determination R^2 and smallest standard error SE) was selected. Jahan and Gan (2011) found a nonlinear model type [Eq. (5)] to predict NDVI of forest from climatic variables. In this study, both linear [Eq. (4)] and nonlinear [Eqs. (5)–(7)] models were

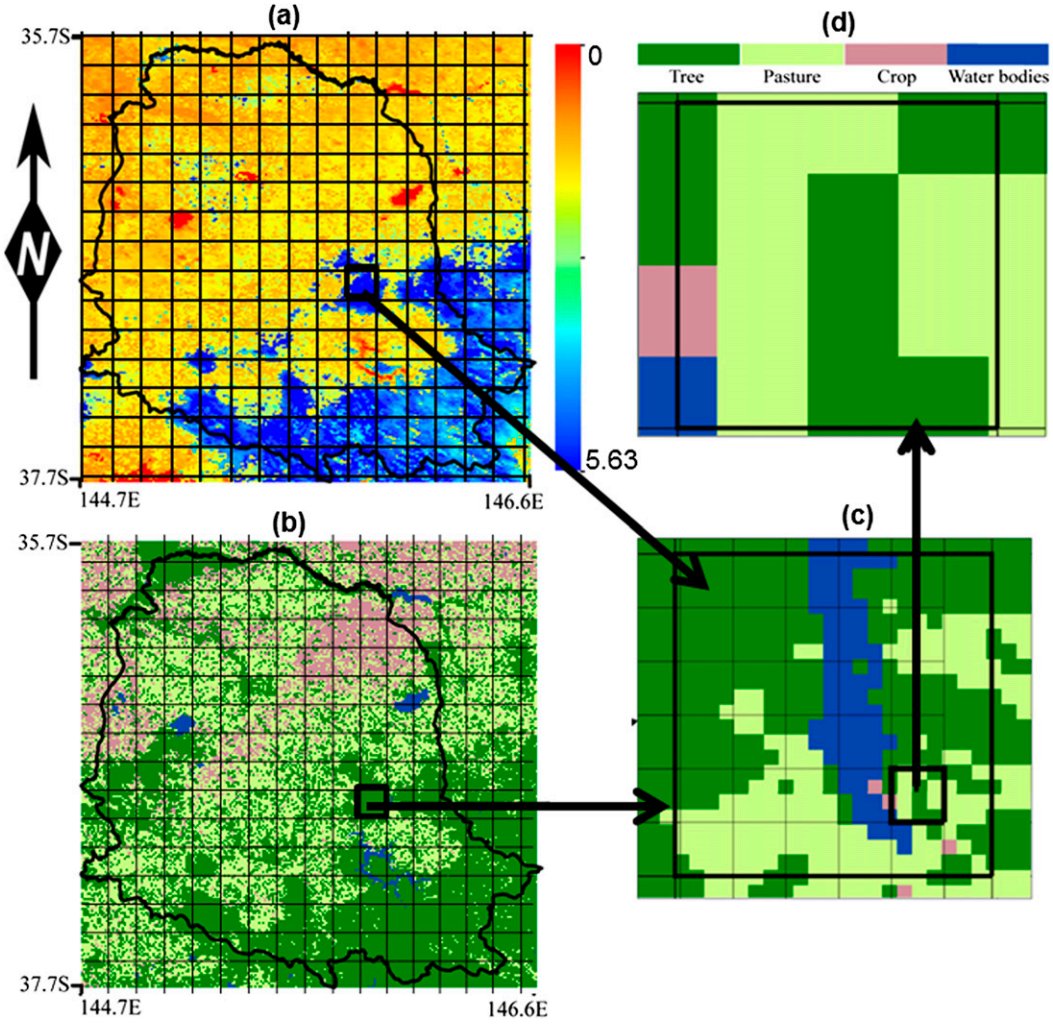

FIG. 3. (a) The spatial alignment of LAI pixels with the AWAP, (b) the spatial alignment of land cover type (tree, pasture, crop, and water bodies) pixels with the AWAP grid, (c) land cover types with both the AWAP climate pixel grid (large rectangle) and MODIS LAI pixel grid (small rectangles) shown, and (d) the spatial alignment of land cover types inside the MODIS LAI pixel.

assessed to relate LAI and climate for annual and monthly time scales:

$$\mathrm{LAI} = \alpha_0 + \alpha_1 X_1 + \alpha_2 X_2, \tag{4}$$

$$\mathrm{LAI} = \alpha_0 + \alpha_1 X_1^{\alpha_2} + \alpha_3 X_2^{\alpha_4}, \tag{5}$$

$$\mathrm{LAI} = \alpha_1 \times X_1^{\alpha_2} \times \alpha_3^{X_2}, \quad \text{and} \tag{6}$$

$$\mathrm{LAI} = \frac{\alpha_1}{1 + \exp[-(X_1 - \alpha_2)/\alpha_3]}, \tag{7}$$

where α_0, α_1, α_2, α_3, and α_4 are model parameters that need to be calibrated and X_1 and X_2 are climate predictors (precipitation, reference crop evapotranspiration, mean temperature, and moisture state). For crop and pasture 6-month moving-averaged P, PET and T were used as predictors, whereas for tree 9-month moving-averaged P, PET and T were used (either individually or combined together), while the monthly LAI was used as the predictand. Calibration of the model parameters was based on the period (2000–04) to minimize the root-mean-square error between the modeled LAI and the remotely sensed BNU MODIS LAI in a least squares framework. Data from 2005 to 2009 were used to validate the calibrated models. The *t*-test statistic was used to test whether or not the model parameters were statistically different from zero. During a preliminary analysis, the best performing models from the available combinations of climate variables were selected. The spatial predictability of the monthly LAI of each land cover type from the spatial

TABLE 1. The four representative concentration pathways (reproduced from Moss et al. 2010).

RCPs	Radiative forcing	Concentration (ppm)	Pathway
RCP8.5	>8.5 W m^{-2} in 2100	>1370 CO_2 equivalent in 2100	Rising stabilization without
RCP6.0	~6 W m^{-2} at stabilization after 2100	~850 CO_2 equivalent (at stabilization after 2100)	Overshoot stabilization without
RCP4.5	~4.5 W m^{-2} at stabilization after 2100	~650 CO_2 equivalent (at stabilization after 2100)	Overshoot
RCP2.6	Peak at ~3 W m^{-2} before 2100 and then declines	~490 CO_2 equivalent before 2100 and then declines	Peak and decline

variable precipitation and reference evapotranspiration were represented using the spatial distribution of R^2 for each BNU MODIS LAI pixel. The coefficient of determination between predicted monthly LAI using the nonlinear model type [Eq. (7)] and observed monthly LAI from the BNU MODIS were calculated for each BNU MODIS LAI pixel. Each BNU MODIS LAI pixel has 120 months from 2000 to 2009 and the same number of modeled LAI based on a nonlinear relationship with moisture state.

d. Preparing climate model output

Climate projections from the Coupled Model Intercomparison Project phase 5 (CMIP5) Global Climate Model (GCM), used in the Intergovernmental Panel on Climate Change (IPCC) Fifth Assessment Report, are used in this study to assess potential climate change impacts on LAI. Four representative concentration pathways (RCPs) provide radiative forcing scenarios over the twenty-first century. Further information on the development and design of the RCPs can be found in Moss et al. (2010) and van Vuuren et al. (2011). Each RCP is suffixed with its estimated radiative forcing value at the end of the twenty-first century relative to the preindustrial value. For example, the acronym RCP8.5 indicates that radiative forcing increases throughout the twenty-first century to a maximum of 8.5 W m^{-2} at the end of the century (see Table 1) for more details.

To assess the impacts of future climate change on LAI in the Goulburn–Broken catchment, the averages from the 30 different climate model outputs from CMIP5 GCM (http://climexp.knmi.nl/) were statistically downscaled using the delta change method. One of the advantages of using this method is that an observed database is used as the baseline, resulting in a consistent set of scenario data. The study area is covered by four (2.5° × 2.5°) CMIP5 GCM climate model pixels, so the area-weighted average precipitation and mean temperature were used for estimating the delta values:

$$T_{\Delta}(j) = T_{\text{obs}}(j) + \Delta_T(j) \quad \text{and} \tag{8}$$

$$\Delta_T(j) = \overline{T}_{\text{projn}}(j) - \overline{T}_{\text{control}}(j), \tag{9}$$

where T_{Δ} is the downscaled monthly temperature for a climate change scenario simulation, $T_{\text{obs}}(j)$ is the observed temperature in the historical period (1981–2010) for month j, and $\Delta_T(j)$ is the change in the 30-yr mean temperature as projected by the climate model $\overline{T}_{\text{projn}}(j)$ for three future periods (2011–40, 2041–70, and 2071–2100) relative to the control (1981–2010) climate model simulation $\overline{T}_{\text{control}}(j)$. The delta change method for precipitation can be described by the following equations:

$$\Delta_P(j) = \frac{\overline{P}_{\text{projn}}(j)}{\overline{P}_{\text{control}}(j)} \quad \text{and} \tag{10}$$

$$P_{\Delta}(j) = P_{\text{obs}}(j) \times \Delta_p(j), \tag{11}$$

where P_{Δ} is the downscaled monthly precipitation for the projected future climate change scenario, $P_{\text{obs}}(j)$ is the observed monthly precipitation in the historical period (1981–2010) for month j, and $\Delta_P(j)$ is the change in 30-yr mean precipitation as simulated by the climate model $\overline{P}_{\text{projn}}(j)$ for three future periods (2011–40, 2041–70, and 2071–2100) relative to the control simulation $\overline{P}_{\text{control}}(j)$. For future climate scenarios, the PET was computed using the projected minimum and maximum temperature, keeping the other input (wind speed, actual vapor pressure, and solar radiation) the same as the historical observation during 1981–2010.

3. Results and discussions

a. Relationship between annual LAI and climatic variables

Based on the lumped annual LAI and annual precipitation, annual reference crop evapotranspiration, and moisture state, relationships were investigated for the whole period 2000–09. A strong linear relationship (R^2 = 0.70) was found between the average annual LAI of crop and mean annual precipitation (Fig. 4a).

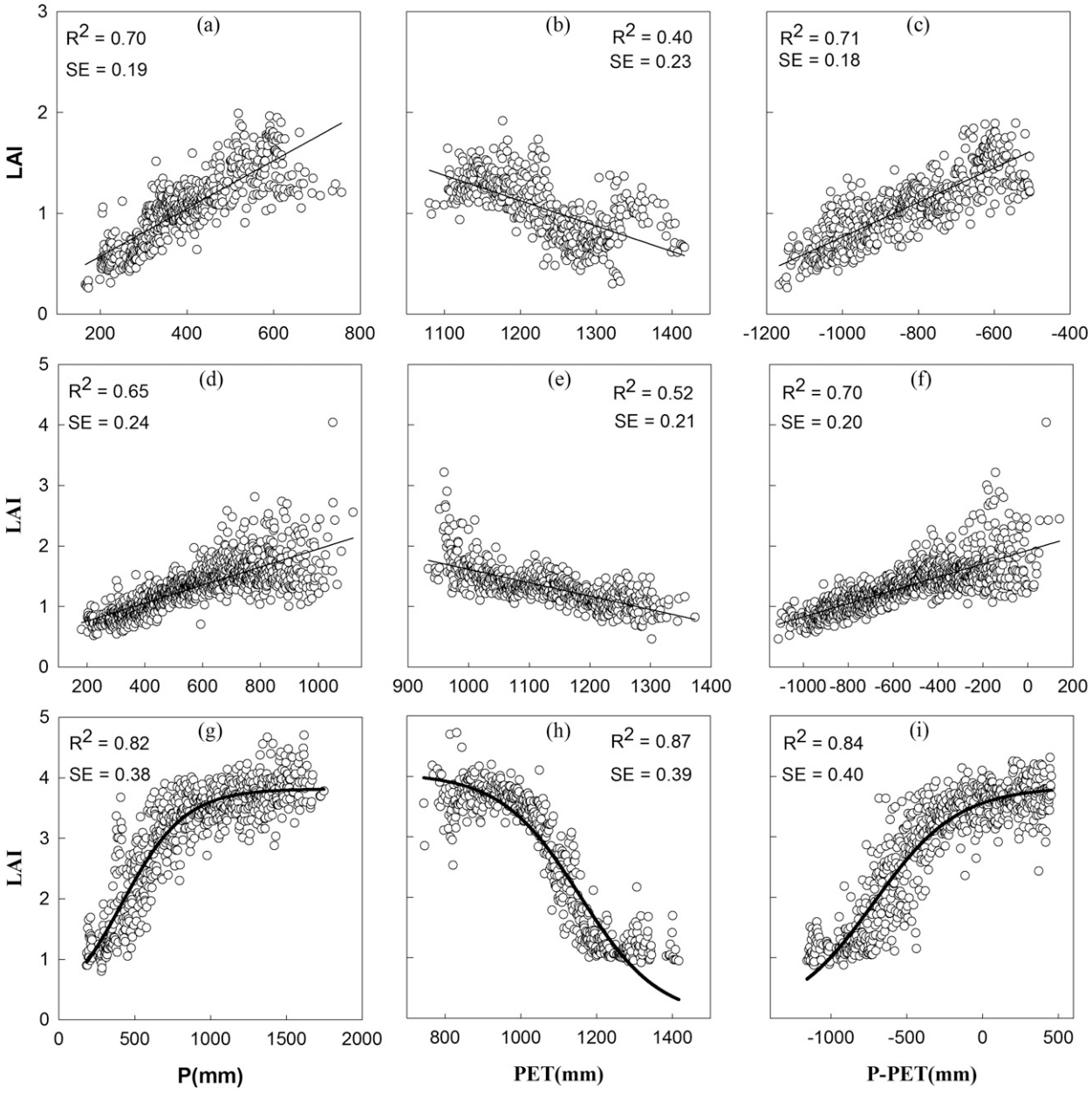

FIG. 4. Annual LAI against annual P, annual PET, and annual P − PET for (a)–(c) crop, (d)–(f) pasture, and (g)–(i) tree, respectively.

The annual LAI of crop showed a weak (R^2 = 0.40) negative relationship with annual reference crop evapotranspiration (Fig. 4b). Some of this weaker relationship is likely due to actual evapotranspiration and plant growth being more strongly controlled by precipitation than potential evapotranspiration, as well as phenological effects like crop growth and harvesting. The annual moisture state (P − PET) showed a strong relationship (Fig. 4c; R^2 = 0.71), but the relationship is strongly influenced by the precipitation term since the relationship with reference crop evapotranspiration alone was weak. The improvement of R^2 from adding the reference crop evapotranspiration was not considerable. The other important point to be considered is that most of the crop in the study area is located in the semiarid parts of the catchment, where plant growth is strongly controlled by the availability of water rather than energy, as available energy is far in excess of available water (Zhang et al. 2004).

The annual LAI of pasture is also linearly related to the annual precipitation, annual reference crop evapotranspiration, and the annual moisture state (P − PET)

TABLE 2. Result of model parameter calibration for both linear and nonlinear models with R^2 and SE for the whole period (2000–09) of annual and (2000–04) of monthly analysis. Precipitation parameters for the nonlinear model [Eqs. (5) and (6)] are in bold.

				Model parameters						
Model type	Cover type	Predictors	Time scale	α_0	α_1	α_2	α_3	α_4	R^2	SE
Linear [Eq. (4)]	Crop	P	Annual	0.098	0.002	—	—	—	0.70	0.19
	Crop	PET		4.140	−0.003	—	—	—	0.40	0.23
	Crop	P − PET		2.475	0.002	—	—	—	0.71	0.18
	Pasture	P		0.460	0.002	—	—	—	0.65	0.24
	Pasture	PET		3.829	−0.002	—	—	—	0.52	0.21
	Pasture	P − PET		1.926	0.001	—	—	—	0.70	0.20
Nonlinear [Eq. (7)]	Tree	P		—	3.816	208.739	412.334	—	0.82	0.38
	Tree	PET		—	4.051	−104.631	1155.805	—	0.87	0.39
	Tree	P − PET		—	3.822	277.037	−716.967	—	0.84	0.40
Nonlinear [Eq. (5)]	Crop	P, T	Monthly	21.6017	**0.0002**	**2.0232**	−15.8444	0.1020	0.88	0.28
	Pasture	P, T		−24.0027	**0.0082**	**1.1243**	28.3731	−0.0534	0.78	0.31
	Tree	P, T		−45.5570	**46.8648**	**0.0186**	−4.3495	−0.3275	0.43	0.44
Nonlinear [Eq. (6)]	Crop	P, T		—	0.440	**0.833**	0.861	—	0.85	0.29
	Pasture	P, T		—	0.412	**0.536**	0.937	—	0.75	0.32
	Tree	P, T		—	0.603	**0.321**	1.022	—	0.45	0.44
Nonlinear [Eq. (7)]	Crop	P − PET		—	136.484	159.456	42.561	—	0.93	0.25
	Pasture	P − PET		—	6.250	43.616	62.616	—	0.95	0.20
	Tree	P − PET		—	4.209	−57.185	36.948	—	0.95	0.25

over the study region from 2000 to 2009. Like cropped areas, the annual precipitation showed the higher control on the annual LAI of pasture (Fig. 4d) than annual reference crop evapotranspiration (Fig. 4e). The possible reason for this weak relationship with annual reference crop evapotranspiration is the same as that of crop stated above.

Unlike a linear relationship of crop and pasture, the annual LAI of tree showed a strong ($R^2 = 0.82$) positive nonlinear relationship with annual precipitation (Fig. 4g) and annual moisture state (Fig. 4i). The annual LAI also showed strong ($R^2 = 0.87$) negative nonlinear relationships with annual reference crop evapotranspiration (Fig. 4h). From the scatterplot of tree, the response of the annual LAI of tree to annual precipitation is stronger for trees where annual precipitation is below 1000 mm. Trees receiving annual precipitation above 1000 mm showed less sensitivity to change in annual precipitation. All model parameters for the annual LAI are statistically different from zero ($p < 0.001$) for all cover types and are provided in Table 2.

b. *Relationship between monthly LAI and climatic variables*

In a preliminary analysis (Table 2), the four models in Eqs. (4)–(7) were compared with the aim of selecting a single model that uses lumped monthly LAI. The nonlinear models Eqs. (5) and (6) could predict the monthly LAI of crop and pasture but were poor for tree. The monthly LAIs of each land cover type were regressed against combinations of the 6- and 9-month moving average climatic variables for all years (2000–04). The nonlinear model Eq. (5) performed similarly to nonlinear model Eq. (6), except in predicting negative LAI via the intercept term. Hence, Eq. (6) avoided this problem and performed well for crop and pasture but produced a poor fit for tree (Table 2). The models worked best when forced by precipitation and temperature out of all the various possible climatic variable combinations. The model parameters based on the period (2000–04) of analysis are shown in Table 2. The model for the entire period (2000–09) for crop performs well ($R^2 = 0.85$), as does the pasture model ($R^2 = 0.75$), but performs poorly for tree ($R^2 = 0.45$).

The other nonlinear candidate [Eq. (7)] for modeling monthly LAI consistently performed well for all land cover types. The best performance was found when the lumped monthly LAI was regressed against a 6-month moving average for crop and pasture and a 9-month moving average of the moisture state (P − PET). The coefficients of determination of the model calibration for the whole period of study were 0.93, 0.95, and 0.95 (Table 2) for crop, pasture, and tree, respectively. Independent calibration for the period 2000–04 and the validation period 2004–09 were conducted, and the model performance can be considered good with all parameter values statistically significantly different from zero ($p < 0.001$). The calibration and validation of the model are shown in Figs. 5a and 5b for crop, Figs. 5c and 5d for pasture, and Figs. 5e and 5f for tree.

The performance of the calibrated crop, pasture, and tree models, based on [Eq. (7)] and the moving-average

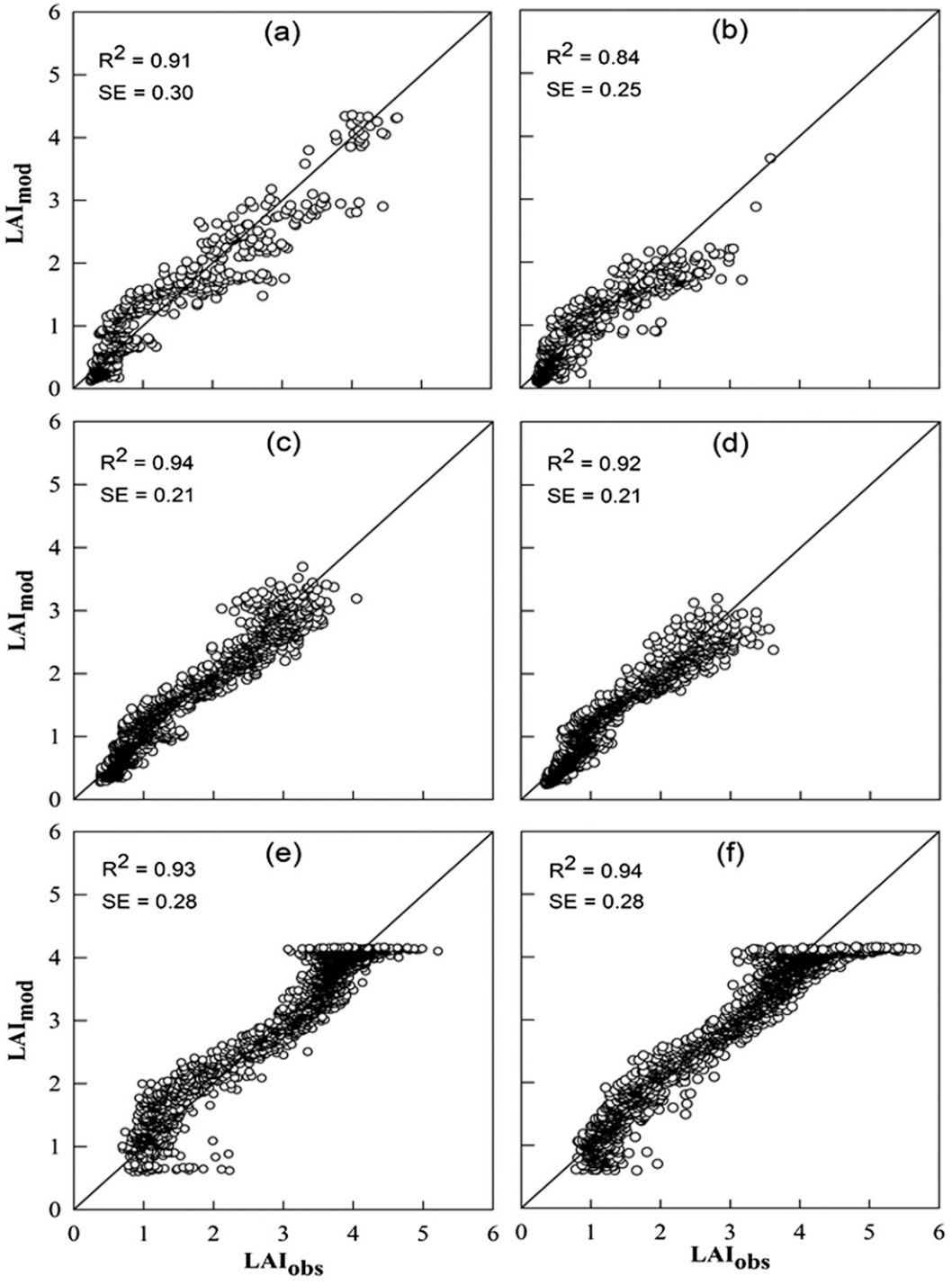

FIG. 5. Monthly LAI against the 6- (crop and pasture) and 9-month (tree) moving average of P − PET: (a),(c),(e) Calibration and (b),(d),(f) validation for crop, pasture, and tree, respectively, using the nonlinear model [Eq. (7)].

moisture state (P − PET), is shown spatially across the catchment through the distribution of R^2 between MODIS monthly LAI and predicted monthly LAI (Fig. 6a). The coefficient of determination range from R^2 = 0.1–0.90. A weak response in LAI is shown when moisture state (P − PET) is less than −100 mm for both crop and pasture. When moisture state increases above this level, the increasing LAI responds as P − PET

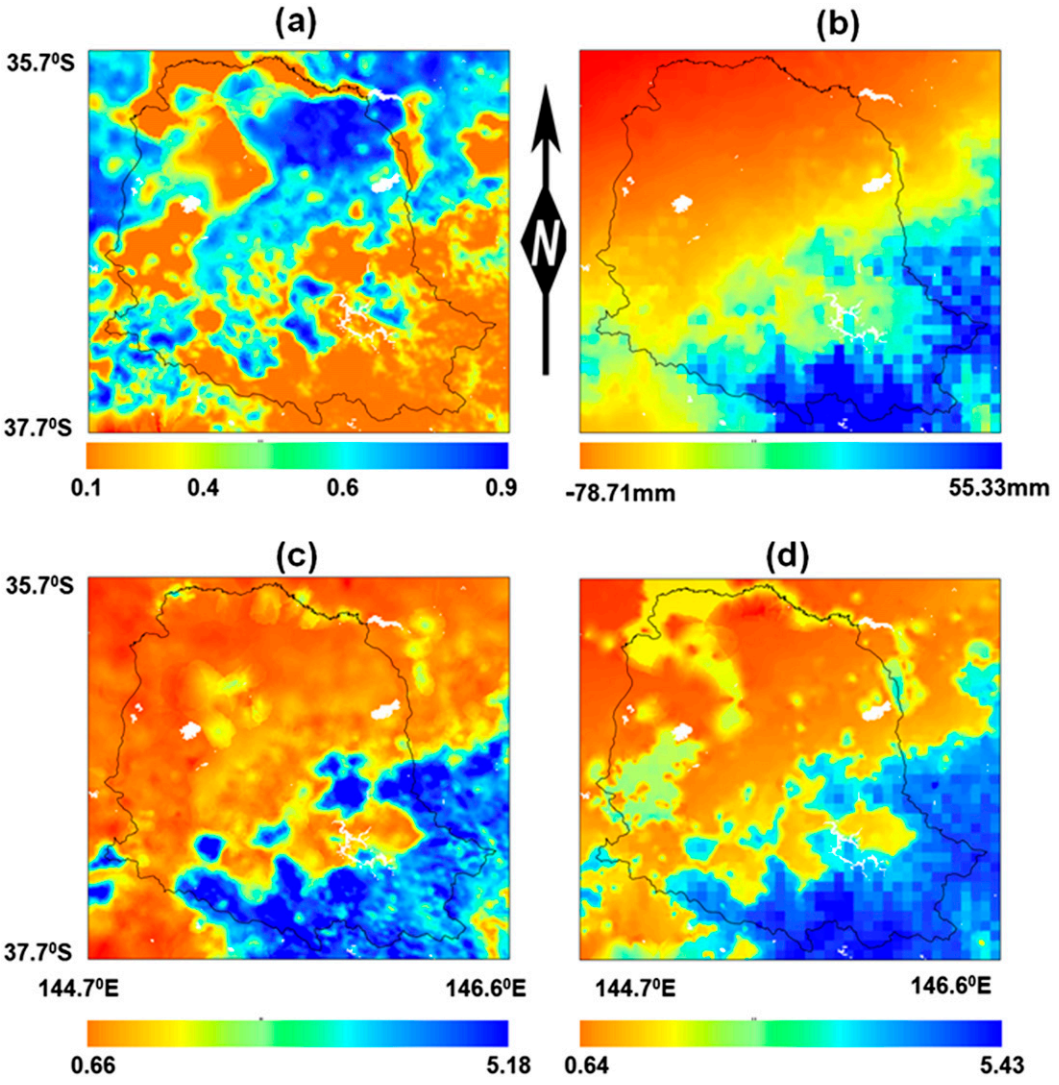

FIG. 6. (a) Spatial distribution of the R^2 between monthly predicted LAI using Eq. (7) and observed LAI from MODIS sensor, (b) average of mean monthly moisture state (P − PET), (c) the observed mean annual LAI from MODIS sensor, and (d) modeled mean annual LAI using Eq. (7), all for the study period (2000–09).

increases. Whereas for tree, monthly LAI is strongly controlled by moisture state (P − PET) below −100 mm, while the relationship between monthly LAI and P − PET flattens for moisture state (P − PET) above −100 mm. The lowest LAI in tree areas was around 1, indicating a perennial canopy is maintained.

The spatial variation in LAI of crop and pasture is well captured in most parts of the catchment but showed low spatial correlation with the moisture state P − PET for tree located in the mountain part of the catchment. Part of the reason is due to with the spatial distribution of moisture state P − PET and where the relationships are strongest for crop and pasture (P − PET > −150 mm) and tree (P − PET < 0 mm). We should also note that our relationships are between bin averages, where we get very high R^2 values, whereas our map (Fig. 6a) of model performance is between observed MODIS pixel values of LAI and our model estimate of a bin-averaged LAI. Where the variance around the bin-averaged LAI is small, we will have a good prediction, and where the variance around the bin-average LAI is large, we will have a poor prediction. The other reason for the good spatial performance of crop and pasture could be related to the flat landscape with little or no access to groundwater storage, whereas most of the trees that are located in the mountain part of the catchment could access the groundwater or soil water storage to buffer the water deficit, as explained by O'Grady et al. 2011 and Thompson

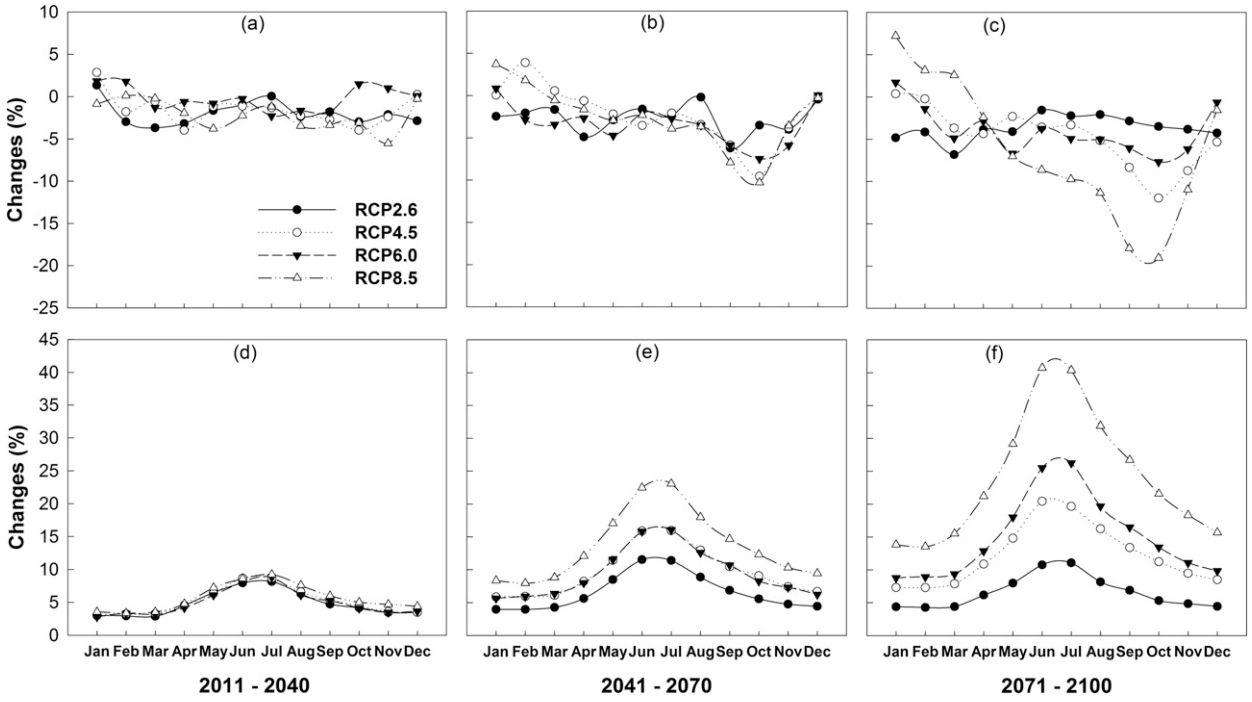

FIG. 7. The percentage change in future (2011–40, 2041–70, and 2071–2100) (a)–(c) mean monthly precipitation and (d)–(f) reference crop evapotranspiration from the historical (1981–2010) mean under the four climate change scenarios.

et al. 2011. The spatial pattern of predicted mean annual LAI showed a good agreement with the spatial pattern of the average of the mean monthly moisture state (P − PET; Figs. 6b,d). The spatial pattern comparison between the observed mean annual LAI from the MODIS sensor (Fig. 6c) with the predicted mean annual LAI (Fig. 6d) from the nonlinear model [Eq. (7)] also showed good agreement. Hence, moisture state dictated the spatial pattern and variability of LAI of crop and pasture and, to some extent, tree.

c. *Assessing climate change impacts on LAI*

The potential impacts of future climate change on the LAI of crop and pasture were assessed using the nonlinear model [Eq. (7)] because the input (precipitation and temperature) required area readily available from the CMIP5 GCM output. The downscaled GCM projections show increases in mean monthly temperature and generally decreases in mean monthly precipitation for the three projected future periods (2011–40, 2041–70, and 2071–2100). Projected changes in mean monthly precipitation (Figs. 7a–c) and reference evapotranspiration (Figs. 7d–f) for the three future periods are shown. A consistent increase in mean monthly temperatures is expected, ranging from 1° to 4°C among the climate scenarios. This will increase the potential evapotranspiration up to 48%, 42%, and 38% from the historical (1981–2010) mean monthly winter potential evapotranspiration in crop, pasture, and tree covers, respectively. Decreases in mean monthly precipitation in autumn and spring are between 5% and 10% and are up to 20% in winter, while increases in mean monthly precipitation in summer are up to 8% in comparison with the historical mean monthly precipitation for all cover types.

As discussed in the previous section, the nonlinear model type of Eq. (7) is the best model from the candidate nonlinear models and was used to assess the impact of climate change on the three land cover types. The simulated monthly LAI of crop, pasture, and tree showed decreases under the four projected scenarios as compared with the historical mean monthly LAI. The mean monthly LAI of crop decreased by 5%–14%, pasture decreased by 3%–9%, and tree decreased by 1%–4% under the lowest CO_2 emission scenario (RCP2.6). For the largest CO_2 emission scenario (RCP8.5), the reduction in crop mean monthly LAI was estimated to vary from 12% to 45% and in pasture from 5% to 32%, while that of tree decreased from 2% to 16%, as shown in Figs. 8a–c, 8d–f, and 8g–i, respectively. Similarly, the mean annual LAI is projected to progressively decrease in all three future periods, under all four climate change scenarios (Table 3). Based on our LAI–moisture state (P − PET) model, crop mean monthly and annual LAI is more sensitive than pasture and tree to projected climate

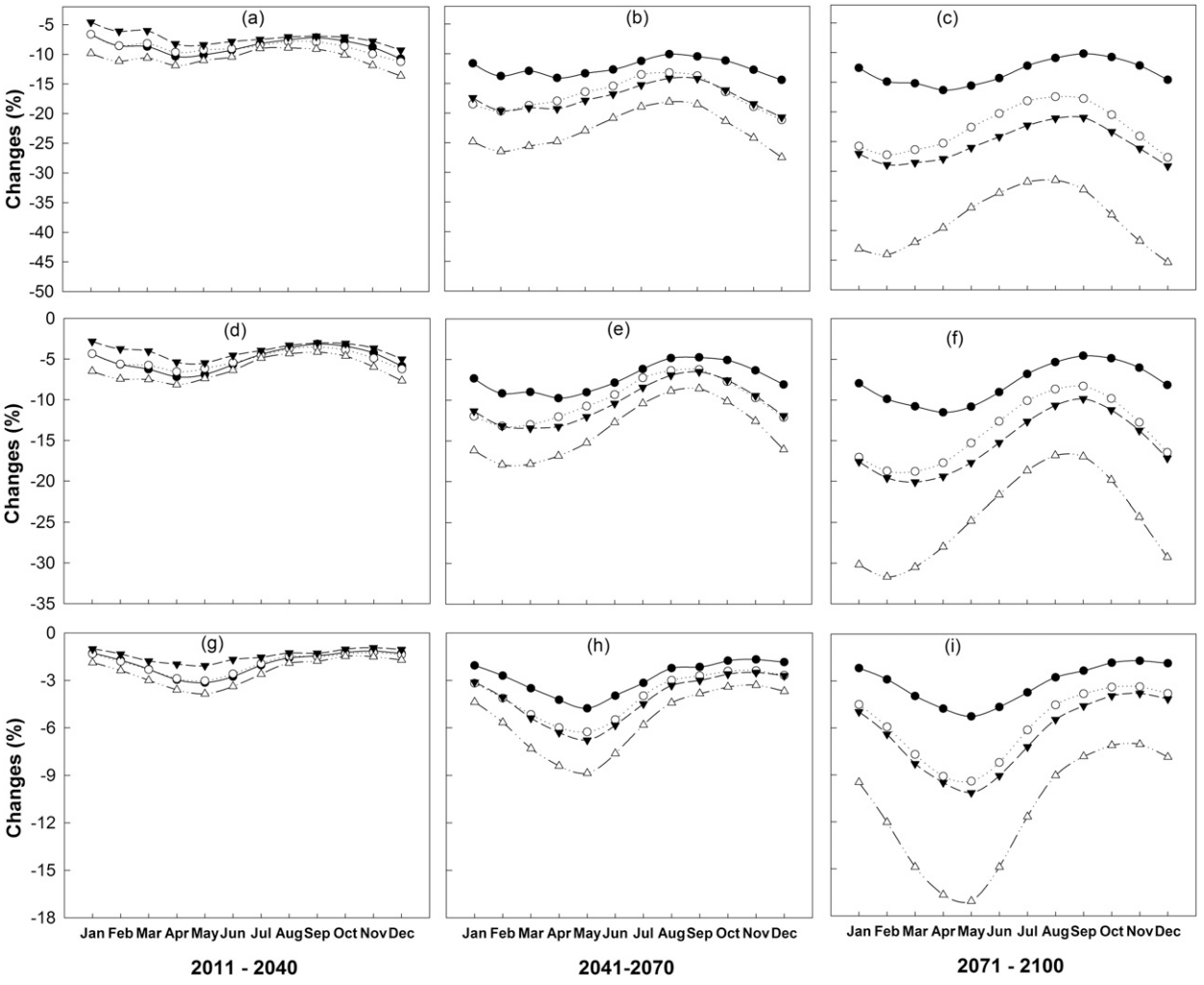

FIG. 8. The percentage change in future (2011–40, 2041–70, and 2071–2100) mean monthly LAI of (a)–(c) crop, (d)–(f) pasture, and (g)–(i) tree from the historical (1981–2010) mean under the four climate change scenarios. The line descriptor legend of Fig. 7 also applies to Fig. 8.

change. The mean monthly and annual LAI of tree was found to be less sensitive.

4. Conclusions

The LAI of vegetation is an important ecohydrological parameter for understanding the dynamic interactions between climate and vegetation and for improving agricultural water management in arid and semiarid areas. This study investigated relationships between LAI of three main land covers (tree, pasture, and crop) in the study region with climate (precipitation, temperature, and reference crop evapotranspiration) through both linear and nonlinear regression models. The results show that both the annual and monthly variations of LAI for all the land cover types are highly related to climatic variations. However, the responses to changes in seasonal and annual climatic variations differed among the land cover types. Of the climatic variables considered, precipitation had the most influence on annual variations in LAI in all land cover types. The moisture state $P - \mathrm{PET}$ was found to drive the seasonal variations of LAI in all land cover types and explained 93%, 94%, and 95% (Table 2) of the seasonal variation of LAI of crop, pasture, and tree, respectively.

The developed models [Eq. (7)] were used to assess possible future climate change impacts on vegetation production in the study region, and the results suggest that under all climate change scenarios, both crop and pasture showed consistent decreases in mean annual LAI in the range of 10%–38% for crop, 5%–24% for pasture, and 2%–11% for tree (Table 3). However, pasture LAI compared to tree LAI was found to be less sensitive to climate change than crop LAI under all climate change

TABLE 3. The percentage change in the mean annual LAI of crop, pasture, and tree as compared to the historical period (1981–2010) for projected climate change under the four RCPs.

	Crop			Pasture			Tree		
RCPs	2011–40	2041–70	2071–2100	2011–40	2041–70	2071–2100	2011–41	2041–70	2071–2100
RCP2.6	−10.65	−13.96	−14.23	−6.05	−8.00	−8.40	−2.31	−3.21	−3.52
RCP4.5	−11.17	−18.22	−22.91	−6.22	−10.44	−13.68	−2.31	−4.28	−6.08
RCP6.0	−9.82	−18.53	−25.75	−5.31	−10.74	−15.21	−1.85	−4.50	−6.70
RCP8.5	−12.63	−23.37	−38.18	−7.20	−13.61	−23.70	−2.82	−5.84	−11.40

scenarios. Furthermore, uncertainty associated with long-term climate projections can be considered by using individual climate model outputs instead of using the mean of all climate model output, as used here. The results can also be used to assess the impacts of future climate and land cover changes on water resources by coupling them with hydrological models, which will assist with assessments of the best land use management options under changing climate. From a hydrologic modeling perspective, considering LAI as a fixed value in hydrologic or land surface modeling of the long-term water balance will lead to overestimation or underestimation of the water balance components (runoff, evapotranspiration, and groundwater recharges) because of the interannual and seasonal variability of LAI in response to climate variables. The findings from this study can be readily coupled with hydrological models to improve the precision of water balance simulations at catchment and continental scales.

Acknowledgments. This work was funded by the Australian Research Council (ARC; Projects ARC LP100100546, ARC LP100100546, and ARC FT120100130), the Natural Science Foundation of China (Project 91125007), and the Commonwealth of Australia under the Australia–China Science and Research Fund (Project ACSRF800). We thank the two anonymous reviewers for excellent and very constructive comments which helped us to improve the manuscript.

REFERENCES

Allen, R. G., L. S. Pereira, D. Raes, and M. Smith, 1998: Crop evapotranspiration: Guidelines for computing crop water requirements. FAO Irrigation and Drainage Paper 56, 300 pp. [Available online at www.fao.org/docrep/X0490E/X0490E00.htm.]

Arora, V. K., 2002a: The use of the aridity index to assess climate change effect on annual runoff. *J. Hydrol.,* **265,** 164–177, doi:10.1016/S0022-1694(02)00101-4.

——, 2002b: Modelling vegetation as a dynamic component in soil-vegetation-atmosphere transfer schemes and hydrological models. *Rev. Geophys.,* **40,** 1006, doi:10.1029/2001RG000103.

Botev, Z. I., J. F. Grotowski, and D. P. Kroese, 2010: Kernel density estimation via diffusion. *Ann. Stat.,* **38,** 2916–2957, doi:10.1214/10-AOS799.

Chamaille-Jammes, S., H. Fritz, and F. Murindagomo, 2006: Spatial patterns of the NDVI-rainfall relationship at the seasonal and inter-annual time scale in an African savanna. *Int. J. Remote Sens.,* **27,** 5185–5200, doi:10.1080/01431160600702392.

Coops, N. C., R. H. Waring, and T. Hilker, 2012: Prediction of soil properties using a process-based forest growth model to match satellite-derived estimates of leaf area index. *Remote Sens. Environ.,* **126,** 160–173, doi:10.1016/j.rse.2012.08.024.

Donohue, R. J., M. L. Roderick, and T. R. McVicar, 2006: On the importance of including vegetation dynamics in Budyko's hydrological model. *Hydrol. Earth Syst. Sci.,* **3,** 1517–1551, doi:10.5194/hessd-3-1517-2006.

Ellis, T. W., and T. J. Hatton, 2008: Relating leaf area index of natural eucalypt vegetation to climate variables in southern Australia. *Agric. Water Manage.,* **95,** 743–747, doi:10.1016/j.agwat.2008.02.007.

Fang, H. L., S. S. Wei, and S. L. Liang, 2012: Validation of MODIS and CYCLOPES LAI products using global field measurement data. *Remote Sens. Environ.,* **119,** 43–54, doi:10.1016/j.rse.2011.12.006.

Fuentes, S., and Coauthors, 2008: An automated procedure for estimating the leaf area index (LAI) of woodland ecosystems using digital imagery, MATLAB programming and its application to an examination of the relationship between remotely sensed and field measurements of LAI. *Funct. Plant Biol.,* **35,** 1070–1079, doi:10.1071/FP08045.

Ge, J., 2009: On the proper use of satellite-derived leaf area index in climate modeling. *J. Climate,* **22,** 4427–4433, doi:10.1175/2009JCLI2868.1.

Geoscience Australia, 2008: GEODATA 9 second digital elevation model (DEM-9S) version 3. Geoscience Australia, Canberra, ACT, Australia, digital media. [Available online at http://www.ga.gov.au/meta/ANZCW0703011541.html.]

Gilgen, A. K., and N. Buchmann, 2009: Response of temperate grasslands at different altitudes to simulated summer drought differed but scaled with annual precipitation. *Biogeosciences,* **6,** 2525–2539, doi:10.5194/bg-6-2525-2009.

Gordon, L., M. Dunlop, and B. Foran, 2003: Land cover change and water vapour flows: Learning from Australia. *Philos. Trans. Roy. Soc. London,* **B358,** 1973–1984, doi:10.1098/rstb.2003.1381.

Graetz, R. D., 1998: The terrestrial carbon pools of the Australian continent: An assessment of their size, dynamics and tractability. Consultancy Report 98/1, CSIRO Earth Observation Centre, Canberra, ACT, Australia, 245 pp.

Groenendijk, M., and Coauthors, 2011: Seasonal variation of photosynthetic model parameters and leaf area index from global Fluxnet eddy covariance data. *J. Geophys. Res.,* **116,** G04027, doi:10.1029/2011JG001742.

Guindin-Garcia, N., A. A. Gitelson, T. J. Arkebauer, J. Shanahan, and A. Weiss, 2012: An evaluation of MODIS 8-and 16-day

composite products for monitoring maize green leaf area index. *Agric. For. Meteor.,* **161,** 15–25, doi:10.1016/j.agrformet.2012.03.012.

Hill, M. J., and Coauthors, 2006: Assessment of the MODIS LAI product for Australian ecosystems. *Remote Sens. Environ.,* **101,** 495–518, doi:10.1016/j.rse.2006.01.010.

Jahan, N., and T. Y. Gan, 2011: Modeling vegetation-climate relationship in a central mixed wood forest region of Alberta using normalized difference and enhanced vegetation indices. *Int. J. Remote Sens.,* **32,** 313–335, doi:10.1080/01431160903464146.

Jones, D. A., W. Wang, and R. Fawcett, 2007: Climate data for the Australian Water Availability Project. Final Rep., National Climate Centre, Australian Bureau of Meteorology, Melbourne, Australia, 36 pp. [Available online at http://143.188.17.20/data/warehouse/brsShop/data/awapfinalreport200710.pdf.]

——, ——, and ——, 2009: High-quality spatial climate data-sets for Australia. *Aust. Meteor. Oceanogr. J.,* **58,** 233–248.

Knyazikhin, Y., J. V. Martonchik, R. B. Myneni, D. J. Diner, and S. W. Running, 1998: Synergistic algorithm for estimating vegetation canopy leaf area index and fraction of absorbed photosynthetically active radiation from MODIS and MISR data. *J. Geophys. Res.,* **103,** 32 257–32 275, doi:10.1029/98JD02462.

——, and Coauthors, 1999: MODIS leaf area index (LAI) and fraction of photosynthetically active radiation absorbed by vegetation (FPAR) product (MOD15). Algorithm theoretical basis document, version 4, 126 pp. [Available online at http://modis.gsfc.nasa.gov/data/atbd/atbd_mod15.pdf.]

McMahon, T. A., M. C. Peel, L. Lowe, R. Srikanthan, and T. R. McVicar, 2013: Estimating actual, potential, reference crop and pan evaporation using standard meteorological data: A pragmatic synthesis. *Hydrol. Earth Syst. Sci.,* **17,** 1331–1363, doi:10.5194/hess-17-1331-2013.

McVicar, T. R., T. G. Van Niel, L. T. Li, M. L. Roderick, D. P. Rayner, L. Ricciardulli, and R. J. Donohue, 2008: Wind speed climatology and trends for Australia, 1975–2006: Capturing the stilling phenomenon and comparison with near-surface reanalysis output. *Geophys. Res. Lett.,* **35,** L20403, doi:10.1029/2008GL035627.

Moss, R. H., and Coauthors, 2010: The next generation of scenarios for climate change research and assessment. *Nature,* **463,** 747–756, doi:10.1038/nature08823.

Negrón Juárez, R. I., H. R. da Rocha, A. M. Silva e Figueira, M. L. Goulden, and S. D. Miller, 2009: An improved estimate of leaf area index based on the histogram analysis of hemispherical photographs. *Agric. For. Meteor.,* **149,** 920–928, doi:10.1016/j.agrformet.2008.11.012.

Nielsen, D. C., J. J. Miceli-Garcia, and D. J. Lyon, 2012: Canopy cover and leaf area index relationships for wheat, triticale, and corn. *Agron. J.,* **104,** 1569–1573, doi:10.2134/agronj2012.0107n.

O'Grady, A. P., J. L. Carter, and J. Bruce, 2011: Can we predict groundwater discharge from terrestrial ecosystems using existing eco-hydrological concepts? *Hydrol. Earth Syst. Sci.,* **15,** 3731–3739, doi:10.5194/hess-15-3731-2011.

Palmer, A. R., S. Fuentes, D. Taylor, C. Macinnis-Ng, M. Zeppel, I. Yunusa, and D. Eamus, 2010: Towards a spatial understanding of water use of several land-cover classes: An examination of relationships amongst pre-dawn leaf water potential, vegetation water use, aridity and MODIS LAI. *Ecohydrology,* **3,** 1–10, doi:10.1002/eco.63.

Peel, M. C., 2009: Hydrology: Catchment vegetation and runoff. *Prog. Phys. Geogr.,* **33,** 837–844, doi:10.1177/0309133309350122.

——, B. L. Finlayson, and T. A. McMahon, 2007: Updated world map of the Köppen-Geiger climate classification. *Hydrol. Earth Syst. Sci.,* **11,** 1633–1644, doi:10.5194/hess-11-1633-2007.

——, T. A. McMahon, and B. L. Finlayson, 2010: Vegetation impact on mean annual evapotranspiration at a global catchment scale. *Water Resour. Res.,* **46,** W09508, doi:10.1029/2009WR008233.

Ramirez-Garcia, J., P. Almendros, and M. Quemada, 2012: Ground cover and leaf area index relationship in a grass, legume and crucifer crop. *Plant Soil Environ.,* **58,** 385–390.

Richard, Y., and I. Poccard, 1998: A statistical study of NDVI sensitivity to seasonal and inter-annual rainfall variations in Southern Africa. *Int. J. Remote Sens.,* **19,** 2907–2920, doi:10.1080/014311698214343.

Sea, W. B., P. Choler, J. Beringer, R. A. Weinmann, L. B. Hutley, and R. Leuning, 2011: Documenting improvement in leaf area index estimates from MODIS using hemispherical photos for Australian savannas. *Agric. For. Meteor.,* **151,** 1453–1461, doi:10.1016/j.agrformet.2010.12.006.

Thompson, S. E., C. J. Harman, A. G. Konings, M. Sivapalan, A. M. Neal, and P. A. Troch, 2011: Comparative hydrology across AmeriFlux sites: The variable roles of climate, vegetation, and groundwater. *Water Resour. Res.,* **47,** W00J07, doi:10.1029/2010WR009797.

van Vuuren, D. P., and Coauthors, 2011: The representative concentration pathways: An overview. *Climatic Change,* **109,** 5–31, doi:10.1007/s10584-011-0148-z.

Wang, J., K. P. Price, and P. M. Rich, 2001: Spatial pattern of NDVI in responses precipitation and temperature in central Great Plains. *Int. J. Remote Sens.,* **22,** 3827–3844, doi:10.1080/01431160010007033.

Wang, Q., S. Adiku, J. Tenhunen, and A. Granier, 2005: On the relationship of NDVI with leaf area index in a deciduous forest site. *Remote Sens. Environ.,* **94,** 244–255, doi:10.1016/j.rse.2004.10.006.

White, D. A., and Coauthors, 2010: Observed and modelled leaf area index in *Eucalyptus globulus* plantations: Tests of optimality and equilibrium hypotheses. *Tree Physiol.,* **30,** 831–844, doi:10.1093/treephys/tpq037.

Yuan, H., Y. Dai, Z. Xiao, D. Ji, and W. Shangguan, 2011: Reprocessing the MODIS leaf area index products for land surface and climate modelling. *Remote Sens. Environ.,* **115,** 1171–1187, doi:10.1016/j.rse.2011.01.001.

Zhang, J., and J. E. Walsh, 2007: Relative impacts of vegetation coverage and leaf area index on climate change in a greener north. *Geophys. Res. Lett.,* **34,** L15703, doi:10.1029/2007GL030852.

Zhang, L., K. Hickel, W. R. Dawes, F. H. S. Chiew, A. W. Western, and P. R. Briggs, 2004: A rational function approach for estimating mean annual evapotranspiration. *Water Resour. Res.,* **40,** W02502, doi:10.1029/2003WR002710.

——, F. F. Zhao, Y. Chen, and R. N. M. Dixon, 2011: Estimating effects of plantation expansion and climate variability on streamflow for catchments in Australia. *Water Resour. Res.,* **47,** W12539, doi:10.1029/2011WR010711.

Zhao, F. F., Z. X. Xu, and L. Zhang, 2012: Changes in streamflow regime following vegetation changes from paired catchments. *Hydrol. Processes,* **26,** 1561–1573, doi:10.1002/hyp.8266.